# Mesoscale Nanoparticles Selectively Target the Renal Proximal Tubule Epithelium

Ryan M. Williams,[†] Janki Shah,[†] Brandon D. Ng,[†] Denise R. Minton,[‡] Lorraine J. Gudas,[§] Christopher Y. Park,[†,⊥] and Daniel A. Heller*,[†,§]

[†]Memorial Sloan Kettering Cancer Center, New York, New York 10065, United States
[‡]Weill Cornell Graduate School of Medical Sciences, New York, New York 10065, United States
[§]Department of Pharmacology, Weill Cornell Medical College, New York, New York 10065, United States
[⊥]Department of Cell and Developmental Biology, Weill Cornell Medical College, New York, New York 10065

**S** *Supporting Information*

**ABSTRACT:** We synthesized "mesoscale" nanoparticles, approximately 400 nm in diameter, which unexpectedly localized selectively in renal proximal tubules and up to 7 times more efficiently in the kidney than other organs. Although nanoparticles typically localize in the liver and spleen, modulating their size and opsonization potential allowed for stable targeting of the kidneys through a new proposed uptake mechanism. Applying this kidney targeting strategy, we anticipate use in the treatment of renal disease and the study of renal physiology.
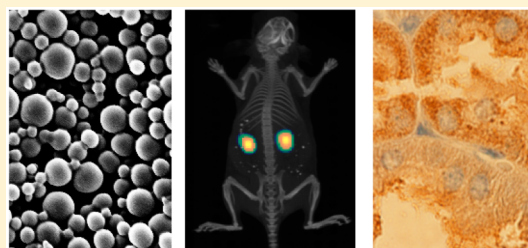
**KEYWORDS:** *Nanotechnology, nanomedicine, targeted drug delivery, controlled release, cancer*

Several kidney diseases may benefit from the development of nanoparticle therapeutics that allow for the site-directed accumulation, controlled temporal release, and protection of a therapeutic payload.[1−3] Among candidate diseases are lupus, glomerulonephritis, and renal cell carcinoma (RCC), which often arises in the proximal tubules.[4−8] Pharmacological therapeutic options for these diseases are limited, thus it is necessary to increase the efficacy and decrease side effects of current drugs.[9,10]

To target specific sites in the body, investigators have taken advantage of specific physiological parameters that enhance delivery to disease sites, including the enhanced permeability and retention (EPR) effect to localize nanoparticles in tumors.[11] In human patients, the EPR effect has not yet been shown to result in significant targeting, however, possibly due to low accumulation in small tumors and disseminated disease.[12,13] Recently, investigators have invested in the "active" targeting of disease sites via functionalization of nanoparticles with a molecular recognition moiety such as an antibody, small molecule or aptamer.[13] This general approach has generated positive preclinical results, some of which have progressed to clinical trials.[13]

Often, and sometimes irrespective of a molecular targeting element, nanoparticles may localize in one of several organs due to the particle surface chemistry, size, and zeta potential.[14,15] The purposeful application of this mechanism may allow for the treatment of diseases regardless of the expression of molecular targets or the size of a lesion. The delivery of targeted agents to specific organs and tissues may obviate off-target effects in systemic delivery such as neutropenia or GI toxicity.[1,16] To employ this targeting approach, it is necessary to understand the properties of nanoparticles that cause differential biodistribution in specific organs and cell types.

To investigate the parameters that may influence nanoparticle localization, we probed the literature and constructed a simple plot to consolidate nanoparticle localization data from multiple studies (Figure 1). We noted the major organ to which the nanoparticles localized as well as the nanoparticle size and the relative degree to which the particle may be opsonized by serum proteins, a natural process that labels exogenous materials for phagocytic destruction by the mononuclear phagocyte system (MPS).[14] Avoidance of MPS-mediated phagocytosis was achieved by nanoparticles with "stealth", or nonopsonizing, materials such as polyethylene glycol (PEG) or natural lipoproteins.[17,18] According to our noncomprehensive survey of the literature, the majority of untargeted nanoparticles primarily accumulate in the liver or spleen. The selective targeting to other organs, including the kidneys or lymph nodes, is rare, although it appears to require a relatively low-opsonizing surface chemistry.[19,20]

Nanomaterial size has a demonstrated effect on biodistribution. Certain synthetic polymers, low-molecular weight proteins, and peptides less than 20 kDa in molecular weight exhibit renal tubule biodistribution but are quickly cleared from the body.[21,22] Nanoparticles less than 250 nm tend to accumulate in the liver or spleen, either through MPS trafficking or entrance through liver fenestrations (approx-
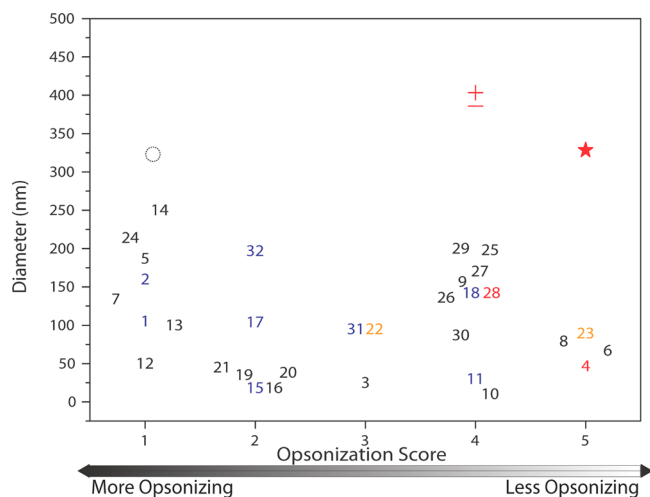
**Figure 1.** Nanoparticle localization reported in the literature. The primary organ of localization for nontargeted nanoparticles administered intravenously to healthy mice was plotted according to the particle diameter and degree of surface passivation. Numbers correlate with literature references listed in Supporting Information Table S1 while the red dash symbol denotes A-MNPs, red plus symbol denotes C-MNPs particles, red star denotes N-MNPs, and black dashed circle denotes O-MNPs synthesized in this study. Black references denote liver localization, blue denotes spleen, red denotes the kidneys, and orange denotes other (stomach or lymph nodes).

imately 100 nm) (Figure 1). Microparticles (particles with diameters above 1000 nm) often localize in the lungs due to entrapment in pulmonary capillary beds.[23−25] Mesoscale nanoparticles refer to the larger gamut of nanoparticles above 100 nm in diameter.[26,27] To date, the long-term biodistribution and tissue localization of mesoscale nanoparticles greater than 250 nm have not been studied in depth.

Herein, we synthesized mesoscale nanoparticles (MNPs) that avoid MPS organs to selectively and stably accumulate in the kidneys up to 7 times more efficiently than other organs. We determined the parameter space required for this localization in terms of particle size and opsonization potential. The nanoparticles accumulated in proximal versus distal renal tubules and more so at their basal rather than the apical membranes. We propose a mechanism in which MNPs are endocytosed by endothelial cells of the peritubular capillaries because of the pressure drop in the nephron and the large absorptive pressure of the capillaries. Applying this targeting strategy, we anticipate that mesoscale nanoparticles could be used to treat diseases that affect the proximal tubules of the kidneys and to study renal blood flow.

**Nanoparticle Synthesis, Characterization, and Biodistribution Studies.** Poly(lactic-co-glycolic acid) conjugated to polyethylene glycol (PLGA−PEG) was synthesized similarly to previously described methods with modifications.[28] Carboxylic acid-terminated poly(lactic-co-glycolic acid) (PLGA) (50:50; MW 38−54 kDa) (90−130 $\mu$mol) (Aldrich; St. Louis, MO) was dissolved in 10 mL of methylene chloride and activated with N-hydroxysuccinimide (NHS, 135 mg, 1.2 mmol) (Aldrich) and 1-ethyl-3-(3-(dimethylamino)propyl)-carbodiimide (EDC, 230 mg, 1.2 mmol) for 30 min with stirring. Conjugated PLGA-NHS was precipitated with 5 mL of ethyl ether, washed 3× with cold 50:50 ethyl ether/methanol, and dried under vacuum. To PLGA-NHS (1g, 18−26 $\mu$mol) in 4 mL of chloroform, 250 mg (50 $\mu$mol) of NH$_2$-PEG-COOH

(MW 5 kDa) (Nanocs; New York, NY) was added with 28 mg (220 $\mu$mol) of N,N-diisopropylethylamine. After the reaction proceeded with mixing overnight, conjugated PLGA−PEG was precipitated and washed 3× with 5 mL of cold methanol and allowed to dry under vacuum. The polymer was characterized by ¹H NMR as previously described.[28]

PLGA−PEG was used to form anionic mesoscale nanoparticles (A-MNPs) by the nanoprecipitation method similarly to as previously described with modifications.[28] PLGA−PEG (100 mg) was dissolved with the fluorescent Cy5 mimic 3,3′-diethylthiadicarbocyanine iodide (DEDC) (Acros Organics; Geel, Belgium) (10 mg) in 2 mL acetonitrile. This solution was added dropwise to 4 mL of water with 100 $\mu$L of 10% Pluronic F-68 (Gibco; Grand Island, NY) and stirred for 2 h. The solution was then centrifuged for 15 min at 6600 rpm, washed, and centrifuged again. Particles were lyophilized in a 2% sucrose solution for storage at −20 °C. Dried particles were suspended in phosphate-buffered saline (PBS) or water and analyzed for size by dynamic light scattering (DLS) (Malvern; Worcestershire, United Kingdom) and scanning electron microscopy (SEM) following gold−palladium coating (Zeiss; Oberkochen, Germany), for $\zeta$-potential by electrophoretic light scattering (ELS) (Malvern), and for encapsulation by UV−vis absorbance (Jasco; Easton, MD) and DEDC fluorescence (Tecan; Mannedorf, Switzerland). To synthesize cationic mesoscale nanoparticles (C-MNPs), 9.5 mg of lyophilized A-MNPs were suspended in a 1 mL solution of 0.5 mg/mL of didodecyldimethylammonium bromide (DMAB) as previously described.[29,30] This method was used by others to modify an anionic PLGA−PEG nanoparticle surface, resulting in cationic nanoparticles functionally shown to be stable for in vitro and in vivo applications.[31−33] Before use, both A-MNPs and C-MNPs were centrifuged and resuspended in PBS to remove unincorporated dye and/or DMAB.

All experiments performed in animals were approved by and carried out in accordance with the MSKCC Institutional Animal Care and Use Committee. Female 4−8 week SKH-1 Elite hairless mice (Crl:SKH1-Hr$^{hr}$) (Charles River; Troy, NY) were used in order to reduce background autofluorescence or absorbance from haired mice. They were fed irradiated 5 V75 alfalfa-free food (LabDiet; St. Louis, MO) to reduce fluorescent background in imaging. Groups of six mice each were injected intravenously via the tail vein with 50 mg/kg of A-MNPs or C-MNPs encapsulating DEDC. Control groups of four mice each were injected with 100 $\mu$L of PBS or 23 $\mu$g/kg of DEDC in PBS with 0.5% DMSO (equal to the amount of encapsulated dye in particle-injected mice), as has been previously performed.[25,34−36] Mice were imaged dorsally with an IVIS Spectrum Preclinical In vivo Imaging System (PerkinElmer; Waltham, MA) using 640 nm excitation and 680 nm emission filters to determine fluorescence biodistribution at the following times postinjection: 30 min, 4 h, and 1−7 days. In vivo fluorescence images were analyzed using Living Image Software v4.3 (PerkinElmer) with regions of interest (ROIs) selected around each kidney and the central lung region to obtain total fluorescence efficiency (TFE) from each. On day 3, three mice from the A-MNP and C-MNP groups, two mice from the PBS control group, and all four mice from the DEDC control group were euthanized by carbon dioxide overdose. The following organs were harvested and imaged for fluorescence: heart, lungs, kidneys, liver, and spleen. TFE for each organ was obtained and normalized by organ weight to obtain organ-level biodistribution. Normalized organ fluorescence for each group

was averaged and standard deviations obtained. The organs were weighed and fixed with 4% paraformaldehyde (PFA) overnight at 4 °C. One mouse treated with anionic nanoparticles was imaged by fluorescence and X-ray computed tomography (CT) with an IVIS Spectrum CT (PerkinElmer) 1 day following injection. Three-dimensional reconstruction of fluorescent foci around the kidneys was performed with multiple imaging fields and overlaid onto a computed tomographic image of the mouse in order to confirm kidney localization and determine particle distribution throughout the organ.

Fixed organs were dehydrated and paraffin embedded before 5 $\mu$m sections were placed on glass slides. The paraffin was removed and the slides were stained with hematoxylin and eosin (H&E) for basic histology. Another set of slides for immunofluorescence were stained with 4′,6-diamidino-2-phenylindole (DAPI) to stain nuclei of cells and either an anti-CD31 antibody to stain endothelial cells (Dianova, Cat # DIA-310) with concentration of 1 $\mu$g/mL or anti-E-cadherin (BD Bioscience; San Jose, CA; Cat# 610181) with concentration of 5 $\mu$g/mL to stain epithelial cells. For detection, isotype-specific secondary antibodies conjugated to AlexaFluor 488 (Invitrogen; Carlsbad, CA; Cat # T20922) were used at 1:1000 dilution according to manufacturer's instruction. Immunohistochemistry was performed using a Discovery XT processor (Ventana Medical Systems; Tuscon, AZ). The tissue sections were deparaffinized with EZPrep buffer (Ventana Medical Systems), antigen retrieval was performed with CC1 buffer (Ventana Medical Systems) and sections were blocked for 30 min with 10% normal rabbit serum in PBS + 0.1% BSA. Anti-PEG (Abcam; Cambridge, MA; Cat # ab94764, 5ug/mL) antibodies specific to the PEG backbone were applied and sections were incubated for 5 h, followed by a 60 min incubation with biotinylated rabbit antirat IgG (Vector Laboratories; Burlingame, CA; Cat # PK-4004) at 1:200 dilution. The assay was performed with a DAB detection kit (Ventana Medical Systems) according to manufacturer instructions. Slides were counterstained with hematoxylin (Ventana Medical Systems) and coverslipped with Permount (Fisher Scientific; Hampton, New Hampshire).

Slides were imaged with an Olympus IX51 inverted light microscope with slide adapter (Olympus; Center Valley, PA) outfitted with an Olympus DP73 digital color camera and Olympus XM10 monochrome camera. Fluorescent slides were excited with filtered light from a X-Cite 120Q lamp (Lumen Dynamics; Ontario, Canada). Fluorescence images were acquired with appropriate filter cubes for DAPI, AlexaFluor 488, and Cy5 with constant exposure times for each fluorophore and analyzed in ImageJ (National Institutes of Health; Bethesda, MD) with constant brightness values for each.

**Results and Discussion.** We synthesized anionic (A-MNPs) and cationic (C-MNPs) mesoscale nanoparticles, which both measured approximately 400 nm in diameter, from poly(lactic-*co*-glycolic acid) (PLGA) functionalized with PEG. The nanoparticles were loaded with a fluorescent dye for biodistribution studies. Carboxylic acid-terminated PLGA was conjugated to heterobifunctional amine-PEG-carboxylic acid. ^{1}H NMR was performed to confirm conjugation. The nanoprecipitation method was used to form A-MNPs of 386.7 nm in diameter with a $\zeta$-potential of −19.5 mV as determined by dynamic light scattering (DLS) and electrophoretic light scattering (ELS), respectively (Table 1,

**Table 1. Size (DLS) and Surface Charge (Zeta Potential) Data of Dye-Loaded Mesoscale Nanoparticles**

| nanoparticle | diameter | $\zeta$ potential |
|---|---|---|
| anionic mesoscale nanoparticle (A-MNP) | 386.7 ± 18.7 nm | −19.5 ± 0.6 mV |
| cationic mesoscale nanoparticle (C-MNP) | 402.8 ± 23.4 nm | 18.3 ± 1.3 mV |

Supporting Information Figure S1a). We confirmed size and spherical morphology by scanning electron microscopy (SEM) (Figure 2a,b). Discrepancy in sizes as measured by SEM and DLS is attributable to shrinkage of the polymer upon drying and differences between dry and hydrodynamic diameters, the latter of which is measured by DLS.[37−39] Didodecyldimethylammonium bromide (DMAB) was introduced form C-MNPs measuring 402.8 nm in diameter with a 18.3 mV $\zeta$-potential. Both particle formulations encapsulated 2.2 $\mu$g 3,3′-diethylthiadicarbocyanine iodide (DEDC) fluorescent dye per 1 mg of nanoparticles. Additionally, the total fluorescence from each nanoparticle formulation was essentially identical (Supporting Information Figure S1b).

In order to explore nanoparticle stability, we performed aggregation, dye release, and $\zeta$-potential assays. Each particle formulation exhibited similar stability after incubation in PBS for 3 days as shown by particle size measurements (Figure 2c).[40−42] Both nanoparticles were stable in storage conditions for at least 3 days as measured in PBS and in serum for up to 48 h in 100% fetal bovine serum (FBS), at which point they began to aggregate. Upon introducing FBS, both cationic and anionic nanoparticles reached approximately the same $\zeta$-potential, which has been observed previously (Figure 2d).[43] Finally, dye release assays showed similar release kinetics in PBS and FBS (Figure 2e).

The nanoparticles selectively accumulated in the kidneys of mice following intravenous injection. We injected 50 mg/kg of A- or C-MNPs into female SKH-1 mice and imaged the animals daily for up to 7 days and biweekly thereafter for approximately 3 months. Biodistribution was measured by fluorescence in vivo in order to track nanoparticle localization and degradation over time, a widely used method that closely approximates other biodistribution assays.[44−47] Mice treated with MNPs showed no significant weight loss compared to mice treated with dye alone (Supporting Information Figure S2). Nanoparticles localized to both kidneys and the chest region (Figure 3a, Supporting Information Figure S3). Upon organ extraction, to obtain more quantitative biodistribution patterns, we examined fluorescence in various organs; the fluorescence signal was significantly greater in the kidneys than in any other organ analyzed (Figure 3b). The fluorescence emission from the kidneys was greatest at day 3 for C-MNP-treated mice: 5.3 times greater than the next-highest organ, the heart, for A-MNPs and 5.9 times for C-MNPs at day 3. Fluorescence was also greatest in the kidneys at day 7: 4.5 times greater for A-MNPs and 3.7 times greater than the heart for C-MNPs. Combined fluorescence and computed tomography (CT) imaging focused solely on the kidneys of a mouse treated with A-MNPs confirmed kidney localization as well as relatively even distribution throughout the kidneys (Figure 3c,d, Supporting Information Movie S1). Thus, surface charge did not significantly affect the biodistribution of these nanoparticles, which may be explained by the finding that incubation in FBS caused the $\zeta$-potentials of A-MNP and C-MNP nanoparticles to become very similar (Figure 2d). We also
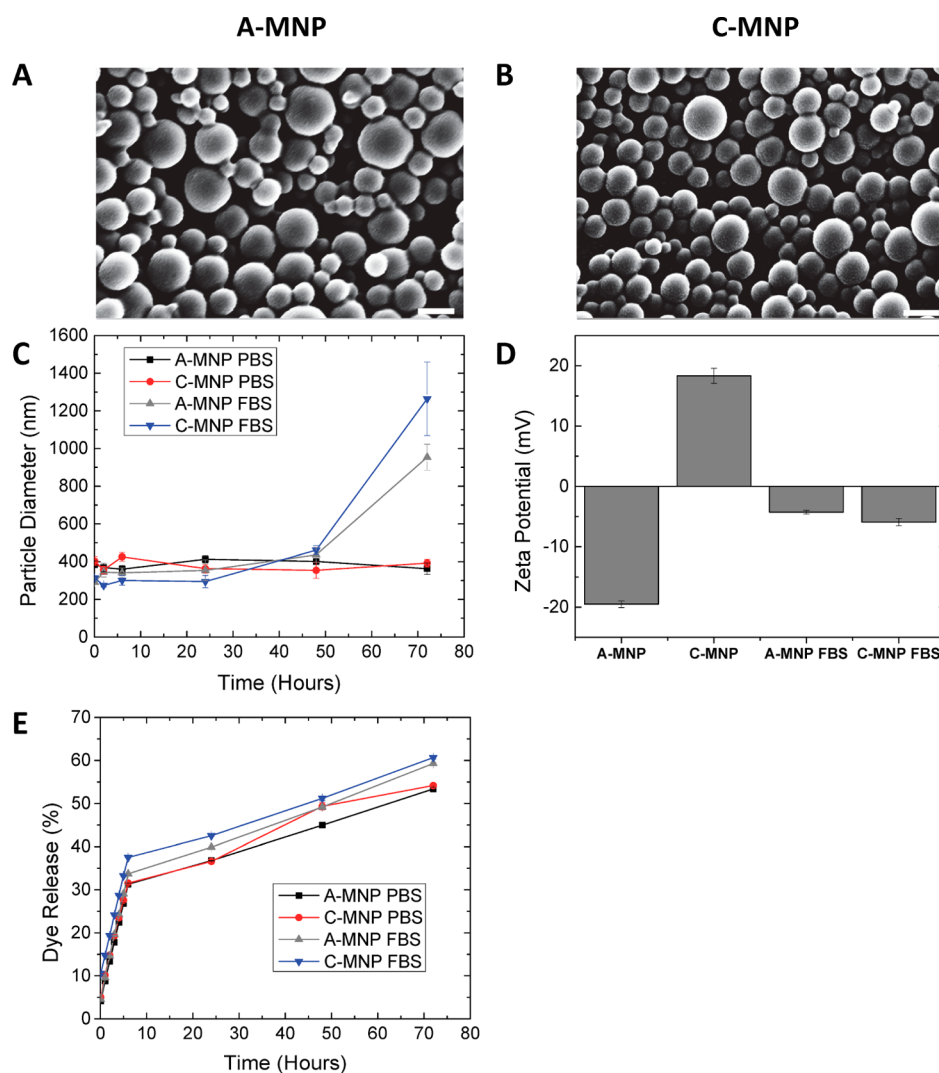
**Figure 2.** MNP characterization. Scanning electron micrographs of (A) A-MNPs and (B) C-MNPs. Scale bars are 300 nm for both images. (C) Dynamic nanoparticle stability measurement by DLS in phosphate-buffered saline (PBS) and fetal bovine serum (FBS). (D) Nanoparticle $\zeta$-potentials in water and FBS. (E) Nanoparticle dye release assay in PBS and FBS.

measured the biodistribution of neutral ($\zeta$-potential = 0.38 mV) mesoscale nanoparticles (N-MNPs), synthesized with methoxy-PEG (mPEG), (Supporting Information Figure S4). These particles, 328.1 nm in diameter, similarly localized preferentially in the kidneys and exhibited 6.7 times more fluorescence than the next-brightest organ, the lungs. We confirmed that surface PEGylation is necessary for kidney localization by determining the biodistribution of non-PEGylated PLGA opsonizing nanoparticles (O-MNPs) with a diameter of 327.1 nm and an anionic surface (−18.1 mV) (Supporting Information Figure S5). These particles primarily localized to the liver 30 min following intravenous injection and appeared to clear by hepatobiliary excretion at 4 h, which we concluded from the nanoparticle localization in the large intestine at this time point. This result correlates with previous research demonstrating that opsonizing nanoparticles are endocytosed by Kupffer cells within the liver within seconds of injection.[48−50] We detected little organ fluorescence above background after 1 day and none after 3 days; thus, surface PEGylation is also necessary for long-term degradation and controlled payload release from the particles, as has been previously described.[18,50] Therefore, MNP kidney targeting

appears to depend predominantly on size and surface functionalization but is independent of moderate surface charges.

Fluorescence imaging in live mice underestimates signal in the kidneys, heart, and other dense tissues compared to ex vivo quantification.[45,51,52] To investigate this difference, we imaged the mouse carcass following organ removal, which revealed a significant decrease in fluorescent foci discussed above (Supporting Information Figure S6a). We determined that the extent to which in vivo imaging underestimates kidney fluorescence is 25−30 times, compared to 2.0−3.5 times for the lungs (Supporting Information Figure S6b).

In order to provide higher order spatial information regarding the distribution of nanoparticles in the kidney, we used both immunofluorescence (IF) and immunohistochemistry (IHC) techniques. Kidney tissue from treated or control mice was sectioned and stained for CD31 (blood vessels) or E-cadherin (distal tubules) expression by IF and for the presence of PEG by IHC. Nanoparticle fluorescence in the renal tubules of MNP-treated mice was significantly higher than negative controls (Figure 4a−c, Supporting Information Figure S7). Furthermore, the fluorescence was brighter in proximal tubules
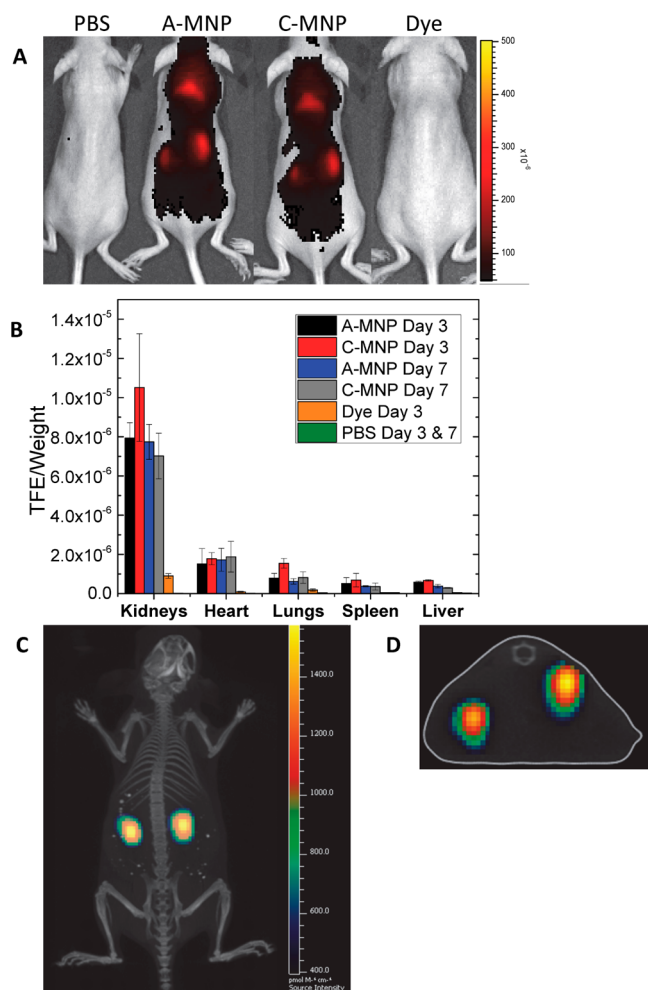
**Figure 3.** In vivo biodistribution of MNPs. (A) Dorsal image of mice treated with PBS, 50 mg/kg A-MNPs, 50 mg/kg C-MNPs, and an equal molar weight of free dye on the day they were sacrificed. (B) Ex vivo organ fluorescence from mice injected with MNPs, dye, or PBS normalized by total organ weight (mean ± SD). (C) Fluorescence plus CT overlay focused on the kidneys of a mouse treated with A-MNPs showing localization and relatively homogeneous distribution throughout the kidneys. (D) Fluorescence plus CT transaxial section of a mouse treated with A-MNPs showing bright fluorescence throughout the kidneys.

compared to distal tubules as revealed by costaining for E-cadherin, a marker of distal tubules (Figure 4a,b,g, Supporting Information Figure S7).[53,54] This tissue distribution pattern was confirmed by antibody staining for PEG (Figure 4e, Supporting Information Figure S9). Thus, colocalized fluorescence from MNPs and staining for the nanoparticle surface confirmed that both the polymer and the encapsulated dye cargo are present in the proximal tubules. Interestingly, there was negligible particle localization in the endothelium or mesangial cells in the glomeruli as determined by IF and IHC (Figure 4d,f, Supporting Information Figures S6 and S9). The fluorescence staining intensity was greater at the basolateral side of the epithelial cells (Figure 4c,h, Supporting Information Figures S7 and 8). In vivo fluorescence dissipated over time (Supporting Information Figure S3), indicating that MNPs target and release payload in a controlled manner in the proximal tubules.

Nanoparticles that selectively and stably localize to the kidneys are relatively rare in the literature (Figure 1). We investigated the parameters necessary to effect localization toward the kidneys and away from other organs such as the liver and spleen. The role of nanoparticle size with respect to the organ of localization is not clear. Also, it is apparent from this study that a relatively small surface charge, or lack thereof, does not significantly affect biodistribution because A-MNPs, C-MNPs, and N-MNPs all localized in the kidneys. Our findings, in agreement with the literature (Figure 1), suggest that the most important factor for directing nanoparticles to organs other than the liver and spleen is a relatively nonopsonizing surface. To this end, Owens and Peppas have suggested that longer PEG chains (>2000 Da) are the most effective at reducing opsonization.[3] Additionally, PEG surface coverage greater than 2% is important.[55] MNPs have 5000 Da PEG chains and a PEG/PLGA weight ratio of 9−13%, suggesting that they will significantly reduce opsonization. Our MNPs have a similar PEG chain size with PEG/PLGA ratios in approximately the same range as others in the literature (Figure 1).

We next probed the mechanism of localization to the kidney at the tissue level. By histology, we showed MNPs predominantly localized in the basolateral region of proximal tubule epithelial cells. Previous work showed that nanoparticles of approximately 80 nm in diameter with a nonopsonizing surface targeted the kidney glomeruli.[19,20] The fenestrations of this segment of the nephron (approximately 80−100 nm[19,56]) are too small for MNPs studied here to pass through, however. There are also fenestrations in the peritubular capillaries which run along the renal tubules; however those are also reportedly too small (∼5 nm) for passage of MNPs.[21] Thus, we propose that our particles were endocytosed by endothelial cells of the peritubular capillaries, which we show to occur in vitro and has been studied previously (Supporting Information Figure S9).[57] It is likely that MNPs are endocytosed to a greater extent by peritubular endothelial cells than glomerular endothelial cells due to the sharp drop in pressure in this segment of the nephron (50−10 mmHg) and the large absorptive pressure of peritubular capillaries that allows the particles greater opportunity to interact with capillary endothelial cell membranes.[56,58] We propose that MNPs are transcytosed across the thin (<500 nm) endothelial cells, as has previously been described for capillary endothelial cells[59,60] and released into the tubulointerstitium between the capillary and epithelial cells of the tubule. The MNPs would likely then be endocytosed by epithelial cells of the tubule; we showed that this occurs in vitro, as previously shown (Supporting Information Figure S10).[61] In these renal epithelial cells, the nanoparticles were retained for days to weeks in mice before degradation. Previous work has shown that PLGA nanoparticles avoid endolysosomal degradation and become associated with the endoplasmic reticulum and Golgi after endocytic uptake,[61] potentially increasing the utility of MNPs for drug delivery in the treatment of diseases affecting the proximal tubules.

In this work, we synthesized and studied a class of polymeric mesoscale nanoparticles that selectively and stably localized in the proximal tubule epithelium of the kidneys. Exploring the parameter spaces responsible for kidney targeting, we found that a low opsonization potential was very important, but moderate changes in zeta potential had no effect on localization. We propose a potential mechanism of localization to the proximal tubules supported by histological evidence whereby the nanoparticles are endocytosed by endothelial cells of the peritubular capillaries because of the pressure drop in the
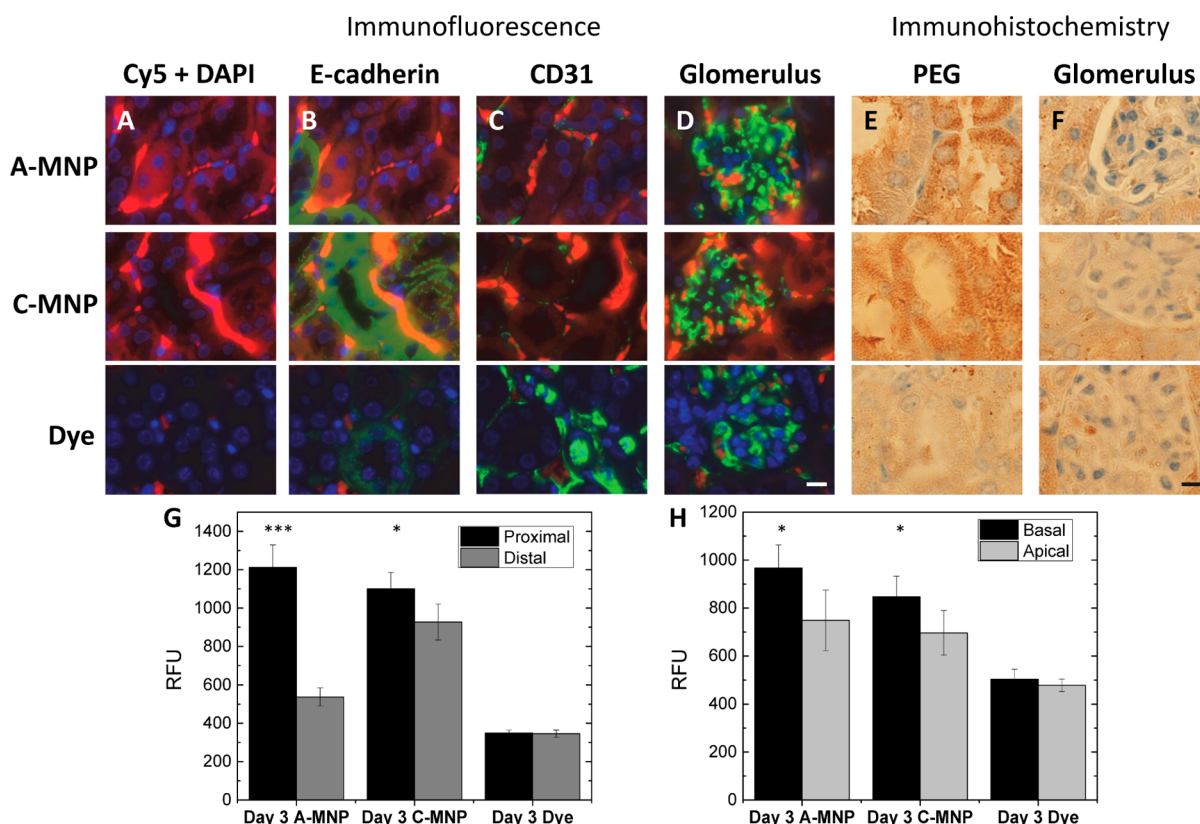
**Figure 4.** Tissue-level localization of MNPs. Representative micrographs of renal tissue from mice at day 3 after nanoparticle administration. (A−D) Immunofluorescence images with blue denoting DAPI stain for cell nuclei and red denoting fluorescence from nanoparticles (excluding bright red blood cells which show standard autofluorescence). Panel A shows fluorescence from nanoparticles and nuclei alone. B shows the same field as A, with green denoting E-cadherin. Green denotes CD31 in C and D. (E,F) Immunohistochemistry with anti-PEG antibody showing particle localization (brown). Panels A−C and E are kidney tubules and panels D and F are glomeruli. (G) Fluorescence quantification in proximal versus distal tubules for each treatment ($n = 5$, mean ± SD). (H) Fluorescence quantification in the basal portion versus apical portion of tubule epithelial cells ($n = 5$, mean ± SD). ***, $p < 0.001$; *, $p < 0.05$. All scale bars denote 10 $\mu$m.

nephron and the large absorptive pressure of the capillaries. However, further study of the physiological mechanism of tissue localization is warranted. This targeting strategy may be applicable to the treatment of diseases that affect the proximal tubules and as a tool for studying renal physiology.

## ASSOCIATED CONTENT

### ⓢ Supporting Information

Further experimental details and Table S1, Figures S1−S10, and Movie S1. This material is available free of charge via the Internet at http://pubs.acs.org.

## AUTHOR INFORMATION

### Corresponding Author
*E-mail: hellerd@mskcc.org. Phone: (646)888-3438.
### Notes
The authors declare no competing financial interest.

## ACKNOWLEDGMENTS

## REFERENCES

(1) Wang, A. Z.; Langer, R.; Farokhzad, O. C. *Annu. Rev. Med.* **2012**, *63*, 185−198.
(2) Peer, D.; Karp, J. M.; Hong, S.; Farokhzad, O. C.; Margalit, R.; Langer, R. *Nat. Nanotechnol.* **2007**, *2*, 751−760.
(3) Owens, D. E., III; Peppas, N. A. *Int. J. Pharm.* **2006**, *307*, 93−102.

(4) Berden, A. E.; Ferrario, F.; Hagen, E. C.; Jayne, D. R.; Jennette, J. C.; Joh, K.; Neumann, I.; Noël, L.-H.; Pusey, C. D.; Waldherr, R. *J. Am. Soc. Nephrol.* **2010**, *21*, 1628−1636.

(5) Fu, L.; Wang, G.; Shevchuk, M. M.; Nanus, D. M.; Gudas, L. J. *Cancer Res.* **2011**, *71*, 6848−6856.

(6) Motzer, R. J.; Bander, N. H.; Nanus, D. M. *New Engl. J. Med.* **1996**, *335*, 865−875.

(7) Wallace, A.; Nairn, R. *Cancer* **1972**, *29*, 977−981.

(8) Bökenkamp, A.; Ludwig, M. *Nephron Physiol.* **2010**, *118*, p1−p6.

(9) Linehan, W. M.; Srinivasan, R. *Nat. Rev. Clin. Oncol.* **2013**, *10*, 614−615.

(10) Gudas, L. J.; Fu, L.; Minton, D. R.; Mongan, N. P.; Nanus, D. M. *J. Mol. Med.* **2014**, *92*, 825−836.

(11) Matsumura, Y.; Maeda, H. *Cancer Res.* **1986**, *46*, 6387−6392.

(12) Prabhakar, U.; Maeda, H.; Jain, R. K.; Sevick-Muraca, E. M.; Zamboni, W.; Farokhzad, O. C.; Barry, S. T.; Gabizon, A.; Grodzinski, P.; Blakey, D. C. *Cancer Res.* **2013**, *73*, 2412−2417.

(13) Bertrand, N.; Wu, J.; Xu, X.; Kamaly, N.; Farokhzad, O. C. *Adv. Drug Delivery Rev.* **2014**, *66*, 2−25.

(14) Almeida, J. P. M.; Chen, A. L.; Foster, A.; Drezek, R. *Nanomedicine* **2011**, *6*, 815−835.

(15) Schroeder, A.; Heller, D. A.; Winslow, M. M.; Dahlman, J. E.; Pratt, G. W.; Langer, R.; Jacks, T.; Anderson, D. G. *Nat. Rev. Cancer* **2011**, *12*, 39−50.

(16) Gradishar, W. J.; Tjulandin, S.; Davidson, N.; Shaw, H.; Desai, N.; Bhar, P.; Hawkins, M.; O'Shaughnessy, J. *J. Clin. Oncol.* **2005**, *23*, 7794−7803.

(17) Alexis, F.; Pridgen, E.; Molnar, L. K.; Farokhzad, O. C. *Mol. Pharmaceutics* **2008**, *5*, 505−515.

(18) Gref, R.; Minamitake, Y.; Peracchia, M. T.; Trubetskoy, V.; Torchilin, V.; Langer, R. *Science* **1994**, *263*, 1600−1603.

(19) Choi, C. H. J.; Zuckerman, J. E.; Webster, P.; Davis, M. E. *Proc. Natl. Acad. Sci. U.S.A.* **2011**, *108*, 6656−6661.

(20) Zuckerman, J. E.; Choi, C. H. J.; Han, H.; Davis, M. E. *Proc. Natl. Acad. Sci. U.S.A.* **2012**, *109*, 3137−3142.

(21) Dolman, M.; Harmsen, S.; Storm, G.; Hennink, W.; Kok, R. *Adv. Drug Delivery Rev.* **2010**, *62*, 1344−1357.

(22) Zhou, P.; Sun, X.; Zhang, Z. *Acta Pharm. Sin. B* **2014**, *4*, 37−42.

(23) Sharma, R.; Saxena, D.; Dwivedi, A. K.; Misra, A. *Pharm. Res.* **2001**, *18*, 1405−1410.

(24) Kim, I.; Byeon, H. J.; Kim, T. H.; Lee, E. S.; Oh, K. T.; Shin, B. S.; Lee, K. C.; Youn, Y. S. *Biomaterials* **2012**, *33*, 5574−5583.

(25) Deshmukh, M.; Kutscher, H. L.; Gao, D.; Sunil, V. R.; Malaviya, R.; Vayas, K.; Stein, S.; Laskin, J. D.; Laskin, D. L.; Sinko, P. J. *J. Controlled Release* **2012**, *164*, 65−73.

(26) Evlyukhin, A.; Kuznetsov, A.; Novikov, S.; Beermann, J.; Reinhardt, C.; Kiyan, R.; Bozhevolnyi, S.; Chichkov, B. *Appl. Phys. B* **2012**, *106*, 841−848.

(27) Yusuf, H.; Kim, W.-G.; Lee, D. H.; Guo, Y.; Moffitt, M. G. *Langmuir* **2007**, *23*, 868−878.

(28) Cheng, J.; Teply, B. A.; Sherifi, I.; Sung, J.; Luther, G.; Gu, F. X.; Levy-Nissenbaum, E.; Radovic-Moreno, A. F.; Langer, R.; Farokhzad, O. C. *Biomaterials* **2007**, *28*, 869−876.

(29) Mei, L.; Sun, H.; Jin, X.; Zhu, D.; Sun, R.; Zhang, M.; Song, C. *Pharm. Res.* **2007**, *24*, 955−962.

(30) Mei, L.; Sun, H.; Song, C. *J. Pharm. Sci.* **2009**, *98*, 2040−2050.

(31) You, J.; Kamihira, M.; Iijima, S. *Cytotechnology* **1997**, *25*, 45−52.

(32) Labhasetwar, V.; Song, C.; Humphrey, W.; Shebuski, R.; Levy, R. J. *J. Pharm. Sci.* **1998**, *87*, 1229−1234.

(33) Song, C.; Labhasetwar, V.; Cui, X.; Underwood, T.; Levy, R. J. *J. Controlled Release* **1998**, *54*, 201−211.

(34) Altınoğlu, E. I.; Russin, T. J.; Kaiser, J. M.; Barth, B. M.; Eklund, P. C.; Kester, M.; Adair, J. H. *ACS Nano* **2008**, *2*, 2075−2084.

(35) Jain, S. K.; Gupta, Y.; Jain, A.; Saxena, A. R.; Khare, P.; Jain, A. *Nanomed. Nanotechnol. Biol. Med.* **2008**, *4*, 41−48.

(36) Xiao, K.; Luo, J.; Fowler, W. L.; Li, Y.; Lee, J. S.; Xing, L.; Cheng, R. H.; Wang, L.; Lam, K. S. *Biomaterials* **2009**, *30*, 6006−6016.

(37) Zhou, J.; Moya, S.; Ma, L.; Gao, C.; Shen, J. *Macromol. Biosci.* **2009**, *9*, 326−335.

(38) Prabha, S.; Zhou, W.-Z.; Panyam, J.; Labhasetwar, V. *Int. J. Pharm.* **2002**, *244*, 105−115.

(39) Reddy, M. K.; Wu, L.; Kou, W.; Ghorpade, A.; Labhasetwar, V. *Appl. Biochem. Biotechnol.* **2008**, *151*, 565−577.

(40) Kievit, F. M.; Wang, F. Y.; Fang, C.; Mok, H.; Wang, K.; Silber, J. R.; Ellenbogen, R. G.; Zhang, M. *J. Controlled Release* **2011**, *152*, 76−83.

(41) Olivier, J.-C.; Vauthier, C.; Taverna, M.; Puisieux, F.; Ferrier, D.; Couvreur, P. *J. Controlled Release* **1996**, *40*, 157−168.

(42) Cui, Z.; Mumper, R. J. *J. Controlled Release* **2001**, *75*, 409−419.

(43) Chung, Y.-I.; Kim, J. C.; Kim, Y. H.; Tae, G.; Lee, S.-Y.; Kim, K.; Kwon, I. C. *J. Controlled Release* **2010**, *143*, 374−382.

(44) Choi, K. Y.; Min, K. H.; Yoon, H. Y.; Kim, K.; Park, J. H.; Kwon, I. C.; Choi, K.; Jeong, S. Y. *Biomaterials* **2011**, *32*, 1880−1889.

(45) Vasquez, K. O.; Casavant, C.; Peterson, J. D. *PLoS One* **2011**, *6*, e20594.

(46) Cai, W.; Shin, D.-W.; Chen, K.; Gheysens, O.; Cao, Q.; Wang, S. X.; Gambhir, S. S.; Chen, X. *Nano Lett.* **2006**, *6*, 669−676.

(47) Faure, A. C.; Dufort, S.; Josserand, V.; Perriat, P.; Coll, J. L.; Roux, S.; Tillement, O. *Small* **2009**, *5*, 2565−2575.

(48) Panagi, Z.; Beletsi, A.; Evangelatos, G.; Livaniou, E.; Ithakissios, D.; Avgoustakis, K. *Int. J. Pharm.* **2001**, *221*, 143−152.

(49) Ogawara, K.-i.; Yoshida, M.; Higaki, K.; Kimura, T.; Shiraishi, K.; Nishikawa, M.; Takakura, Y.; Hashida, M. *J. Controlled Release* **1999**, *59*, 15−22.

(50) Gref, R.; Domb, A.; Quellec, P.; Blunk, T.; Müller, R.; Verbavatz, J.; Langer, R. *Adv. Drug Delivery Rev.* **1995**, *16*, 215−233.

(51) Zou, P.; Xu, S.; Povoski, S. P.; Wang, A.; Johnson, M. A.; Martin, E. W., Jr; Subramaniam, V.; Xu, R.; Sun, D. *Mol. Pharmaceutics* **2009**, *6*, 428−440.

(52) Fujiki, Y.; Tao, K.; Bianchi, D. W.; Giel-Moloney, M.; Leiter, A. B.; Johnson, K. L. *Cytometry, Part A* **2008**, *73*, 11−118.

(53) Prozialeck, W. C.; Lamar, P. C.; Appelt, D. M. *BMC Physiol.* **2004**, *4*, 10.

(54) Piepenhagen, P. A.; Peters, L. L.; Lux, S. E.; Nelson, W. J. *Am. J. Physiol.: Cell Physiol.* **1995**, *38*, C1417.

(55) Gref, R.; Lück, M.; Quellec, P.; Marchand, M.; Dellacherie, E.; Harnisch, S.; Blunk, T.; Müller, R. *Colloids Surf., B* **2000**, *18*, 301−313.

(56) Aird, W. C. *Circ. Res.* **2007**, *100*, 174−190.

(57) Davda, J.; Labhasetwar, V. *Int. J. Pharm.* **2002**, *233*, 51−59.

(58) Brenner, B. M.; Troy, J. L.; Daugharty, T. M. *J. Clin. Invest.* **1971**, *50*, 1776.

(59) Williams, S. K.; Greener, D. A.; Solenski, N. J. *J. Cell. Physiol.* **1984**, *120*, 157−162.

(60) Aird, W. C. *Circ. Res.* **2007**, *100*, 158−173.

(61) Cartiera, M. S.; Johnson, K. M.; Rajendran, V.; Caplan, M. J.; Saltzman, W. M. *Biomaterials* **2009**, *30*, 2790−2798.